machines

MDPI

Article

Open-Switch Fault Detection Based on Open-Winding Five-Phase Fault-Tolerant Permanent-Magnet Motor Drives

Ronghua Cui, Shangshang Yu and Shengquan Li *

College of Electrical, Energy and Power Engineering, Yangzhou University, Yangzhou 225127, China
* Correspondence: sqli@yzu.edu.cn

Abstract: The difficulty of open-switch fault detection in an open-winding inverter is that the fault at the diagonally opposite position within the H-bridge power cell has the same fault characteristics. To solve this problem, this paper proposes an open-switch fault detection method based on open-winding (OW) five-phase fault-tolerant permanent-magnet (FPFTPM) motor drives. The detection method includes three steps: first, the drives open-switch fault is detected by monitoring the component of the third harmonic residual in the stationary reference frame; second, the least squares iterative method based on the forgetting factor is used to identify the relationship between the residual components, which determines the faulty phase and the faulty phase current type; third, an online current injection test method is proposed to accurately identify the open-switch within the H-bridge power cell. Based on the above steps, the open-switch fault at the diagonally opposite position within the H-bridge power cell could be accurately identified. The novelty of the proposed method lies in the possibility that the open-switch fault detection of any switches within the one H-bridge power cell could be accurately achieved by an online current injection test and does not require hardware changes. The experimental results demonstrate the effectiveness of the proposed detection method.

Keywords: open-switch fault detection; open-winding; current-injection test

check for updates

Citation: Cui, R.; Yu, S.; Li, S. Open-Switch Fault Detection Based on Open-Winding Five-Phase Fault-Tolerant Permanent-Magnet Motor Drives. *Machines* **2022**, *10*, 829. https://doi.org/10.3390/machines10100829

Academic Editor: Davide Astolfi

Received: 30 August 2022
Accepted: 19 September 2022
Published: 21 September 2022

Publisher's Note: MDPI stays neutral with regard to jurisdictional claims in published maps and institutional affiliations.

Copyright: © 2022 by the authors. Licensee MDPI, Basel, Switzerland. This article is an open access article distributed under the terms and conditions of the Creative Commons Attribution (CC BY) license (https://creativecommons.org/licenses/by/4.0/).

1. Introduction

Due to environmental pollution and shortage of fossil fuels, electric vehicles (EVs) attract more interest from researchers [1–3]. It is noted that the reliable operation of the motor drives is of crucial significance for EVs because it directly relates to personal safety. Hence, fault-tolerant motor design and fault-tolerant control have been widely investigated [4,5]. The traditional three-phase permanent-magnet synchronous motor (PMSM) drives have poor fault tolerance. Therefore, the performance of the motor system is greatly reduced when there is a fault. In addition, the capacity of the uninterrupted operation without fault is insufficient to meet the high reliability requirements of EVs. Compared with the three-phase PMSM system, the five-phase fault-tolerant permanent-magnet (FPFTPM) motor drives have the superior performance of phase number redundancy, strong fault tolerance, and high reliability. Moreover, through the reliability design rules, FPFTPM can effectively reduce the electrical, magnetic, and thermal coupling between phases [6,7]. Furthermore, when the neutral point of the FPFTPM motor windings is open, each phase winding adopts the H-bridge power supply to form open-winding (OW) FPFTPM motor drives. This can effectively block the fault coupling between the faulty phase and the healthy phase, which can realize phase-to-phase electrical isolation [8]. In addition, the OW FPFTPM motor drives can be applied in low-voltage large-power transmission, making it become a promising candidate for application to EVs [9,10].

EVs often operate in conditions of humidity, vibration, dust, and electromagnetic interference, resulting in a high failure rate of stator windings, power devices, and sensors [11,12]. Among them, open-switch faults are considered as the most common scenarios.

To meet the fault-tolerant operation requirements of EVs, the premise is to detect the open-switch faults, and to provide detailed information support for the subsequent fault-tolerant control. Up to now, the detection of open-switch faults has been widely researched in the literature [13–15]. In general, there are mainly two approaches used to detect open-switch faults, as follows: voltage-based diagnostics and current-based diagnostics.

The voltage-based detection methods that commonly extract fault features from common-mode voltage [16], zero-sequence voltage [17], collector–emitter voltage [18], and line voltage [19] usually need less time for diagnosis. However, these methods generally require additional detection circuits, sensors, or observers. This will inevitably lead to increased costs. At the same time, the accuracy and robustness of the open-switch fault detection methods will be affected by the complexity of the observer algorithm and its sensitivity to motor parameters. In contrast, the current-based detection methods can make full use of phase current and do not require additional sensors apart from the current sensors that are already provided for the current measurement. Therefore, the work in this paper is carried out mainly based on the current signal of the FPFTPM motor.

With the development of the polyphase motor and the demand for fault detection, many fault detection algorithms of three-phase motors have been transplanted to polyphase motors. Considering the particularity of the polyphase motor, fault detection faces new problems, such as detection and control of variables in harmonic space. The current-based detection methods extract fault features from the fundamental current, the low-order harmonic current, the zero-sequence current [20], and the residual current, etc. The appropriate transformation of the stator current is helpful to extract fault features. In terms of six-phase drives, in [21], the average current Park's vector is chosen for open-switch fault detection, and the fault identification approach can be achieved according to the sign symbol of the current vector. For five-phase drives, in [22], the open-switch fault detection is achieved by establishing the relationship between the fundamental current and the third harmonic current and by monitoring their transient conversion process from healthy to faulty. The detection method that used current signal model identification was presented in [23] and the open-switch fault could be detected in less than a quarter of one period. In addition, in [24,25], original and particular algorithms are proposed for the open-switch fault and open-phase fault detection based on a five-phase PMSM; and the adoption of the normalized variables make the detection method completely independent of operating conditions. Nevertheless, it is not suitable for the open-winding topology applications.

In addition to the voltage-based diagnostics and current-based diagnostics, the fault detection method based on an intelligent algorithm is also a promising diagnosis method. This method mainly includes neural network, wavelet analysis, and fuzzy control [26–28]. The detection method based on an intelligent algorithm has little dependence on the model. However, this method requires a large amount of training data, which is hard to achieve under fault conditions. The open-switch detection approaches are summarized in Table 1. In summary, the existing literature shows that most of the studies focus on the open-switch fault of the star-connected inverter. Due to the distinctiveness of the topological structure of the OW FPFTPM motor drives, the system will show the same behavior when the faulty power switch is diagonally opposite the H-bridge power cell. This brings new problems to the detection and identification of open-switch faults, and thus, the existing open-switch detection methods are inapplicable to the OW FPFTPM drives.

The major contribution of this paper is to propose an online open-switch fault-diagnosis approach using the EMF (Electromotive Force) of the faulty phase and the current injection test, which can detect the faulty phase with an open-switch fault and precisely identify the faulty switch. Moreover, there is no need to reconstruct the hardware of OW FPFTPM motor drives. The proposed detection method can provide sufficient open-switch fault information for the next remedial measures to achieve high reliability of the OW FPFTPM motor drives. This paper is organized as follows. Section 2 presents the description of the OW FPFTPM motor drives and the detailed analysis of the of OW FPFTPM motor drives under open-switch faults. In Section 3, the detailed analysis of the

of OW FPFTPM motor drives under open-switch faults is provided. Next, the detection method is described in Section 3. In Section 4, the experimental results are provided to verify the validity of the detection method for OW FPFTPM motor drives.

Table 1. Summary of detection methods.

Detection Methods	Fault Feature	Shortfalls
voltage-based	common-mode voltage zero-sequence voltage collector–emitter voltage	require additional detection circuits, sensors, or observers
current-based	fundamental current low-order harmonic current zero-sequence current	vulnerable to load, focus on the star-connected inverter
intelligent algorithm	neural network wavelet analysis fuzzy logic	require a large amount of training data, high computational complexity, focus on the star-connected inverter

2. An Analysis of OW FPFTPM Motor Drives Suffering from the Open-Switch Fault

This part first describes the OW FPFTPM motor drives and then analyzes the behavior of the drives after suffering from the open-switch fault.

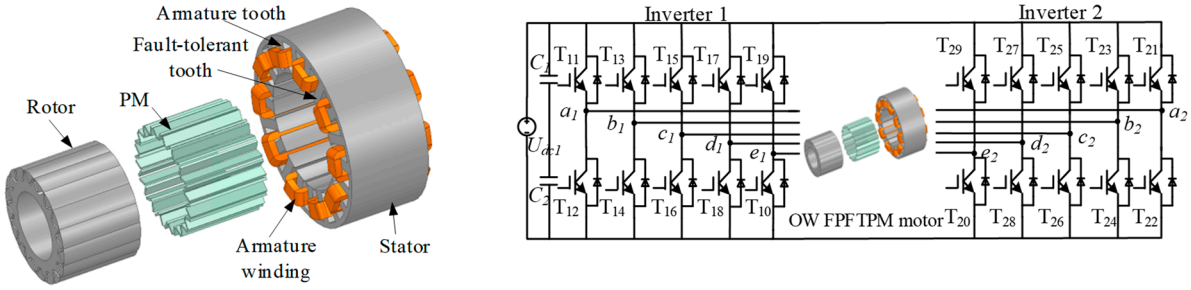
2.1. The Description of OW FPFTPM Motor Drives

The configuration of the FPFTPM motor used in this paper is shown in Figure 1a. The FPFTPM motor is designed as single-layer fractional concentrated winding with the fault-tolerant tooth employed in the stator. Therefore, the stator phase windings have almost no electric, magnetic, and thermal coupling, and the fault-tolerance performance can be greatly improved. The main advantage of the FPFTPM motor is the adoption of the fault-tolerant tooth on the stator, which can also effectively eliminate the influence between faulty phases and other healthy phases. In addition, the self-inductance is almost constant, and the maximum mutual inductance is 0.035 mH (0.259% of the self-inductance). Thus, the mutual inductance and reluctance effects are negligible. The specifications of the FPFTPM motor are listed in Table 2.

Table 2. Specifications of the FPFTPM Motor.

Parameter	Value	Parameter	Value
Rated-phase voltage	100 V	d-axis inductance L_d	13.7 mH
Rated current	4.7 A	q-axis inductance L_q	15.9 mH
Stator resistance	0.5 Ω	Rated speed	1500 r/min
Pole pair	9	DC bus voltage	250 V

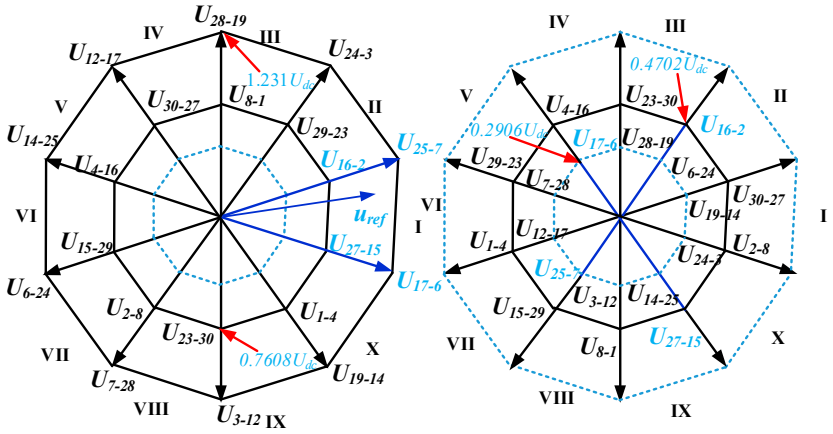
The topology of OW FPFTPM motor drives is shown in Figure 1b. It can be seen from Figure 1b that OW FPFTPM motor drives consist of a common DC bus, an inverter 1 and an inverter 2, and an FPFTPM motor. T_{ij} represents the power switches of the drive, i = 1, 2 denotes the power switches belonging to inverters 1 and 2, and j = 1, 2, 3, 4, and 5, which corresponds to the five phases of the FPFTPM motor, respectively. The OW topology can also effectively eliminate the interaction between the faulty phase and other normal phases, and thereby enhance the reliability of the drives.



(**a**) (**b**)

Figure 1. The OW FPFTPM drives: (**a**) Configuration of the OW FPFTPM motor.; and (**b**) Topology of OW FPFTPM drives.

The two inverters, inverters 1 and 2, are supplied by single DC power $\boldsymbol{U}_{dc}$, therefore, the eliminating common-mode voltage-vectors modulation strategy is adopted. The switch state of $S_i = 1$ means that the upper power switch of the leg, I, is on and the lower power switch is off. $S_i = 0$ means reversely, where i is a_1, b_1, c_1, d_1, e_1, a_2, b_2, c_2, d_2, and e_2. The sequence number of the voltage vectors is the corresponding decimal number of S_i, so 10101 denotes the voltage vector of $\boldsymbol{U_{21}}$, the rest of the voltage vectors and so on. The distribution of the eliminating voltage vectors is shown in Figure 2. When the reference voltage vector $\boldsymbol{u}_{ref}$ is in sector I, as shown in Figure 2, $\boldsymbol{u}_{ref}$ can be generated by the voltage vectors $\boldsymbol{U_{16\text{-}2}}$, $\boldsymbol{U_{17\text{-}6}}$, $\boldsymbol{U_{25\text{-}7}}$, $\boldsymbol{U_{27\text{-}15}}$, $\boldsymbol{U_{0\text{-}0}}$, and $\boldsymbol{U_{31\text{-}31}}$, where the first number represents the voltage vector generated by inverter 1 and the second number denotes the voltage vector generated by inverter 2.



(**a**) (**b**)

Figure 2. Distribution of the voltage vectors. (**a**) α-β plane (ωs); and (**b**) α_3-β_3 plane (ωs).

The space-harmonic magnetomotive force is the direct cause of torque ripple. With the increased number of the phases, the order of the space-harmonic magnetomotive force generated by the fundamental current of the five-phase motor increases. However, the amplitude decreases, which optimizes the torque ripple and improves the efficiency of motor operation. In addition, due to the redundancy of the phase number, when one or two phases of the five-phase motor or the corresponding inverter leg fails, appropriate fault-tolerant control strategies can be adopted to achieve continuous operation of the five-phase motor without restarting or stopping. Therefore, the five-phase motor has strong fault tolerance and high reliability.

2.2. Open-Switch Fault Analysis of OW FPFPTM Motor Drives

It can be seen from section II that each phase winding of FPFTPM motor adopted an independent H-bridge for the power supply. When analyzing the open-switch fault, each

phase can be discussed as a separate unit. Take phase A as an example, according to the faulty switches number within phase A, it can be divided into four groups: a single faulty switch, two faulty switches, three faulty switches, and four faulty switches.

2.2.1. Open-Circuit Fault in the Single Switch

According to Figure 3a, the current following the direction of the arrow is defined as positive. When single open-switch fault occurs in $T_{11,}$ the DC bus fails to provide the positive voltage to the winding and there is only a negative half-cycle current in phase A. Similarly, when single open-switch fault occurs in T_{21} as shown in Figure 3b, the DC bus also fails to provide a negative voltage to the winding, and only a positive half-cycle current exists in phase A. According to symmetry, when T_{12} has an open-switch fault, the behavior of the phase current is the same as T_{21}. Additionally, when T_{22} has an open-switch fault, the behavior of the phase current is the same as T_{11}.

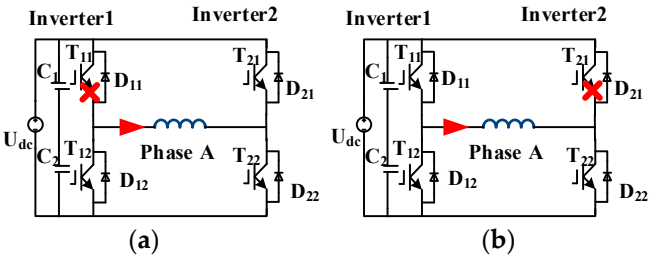


Figure 3. A Single switch with open-circuit faults: (**a**) Open-circuit fault inT_{11}; and (**b**) Open-circuit fault in T_{21}.

2.2.2. Open-Circuit Faults in Two Switches

When two switches have an open-circuit fault in phase A, there are six possible situations in accordance with the location of the open-switch fault. If the two faulty switches are not diagonally opposite, which includes the open-circuit fault in T_{11}, T_{21} or T_{11}, and T_{12}, then the DC bus voltage cannot provide energy for phase A. Consequently, there is no current in phase A. Similarly, the same occurs for the situations when there is an open-circuit fault in T_{12}, T_{22} or T_{21}, and T_{22}. However, when the open-circuit fault occurs at diagonally opposite T_{11} and $T_{22,}$ as shown in Figure 4a, the DC bus can also provide negative voltage to the windings through T_{21} and T_{12}, resulting in a negative half-cycle current in phase A. Likewise, when there are open-circuit faults in T_{21} and $T_{12,}$ as displayed in Figure 4b, the DC bus can still provide positive voltage to the windings through T_{11} and T_{22}, so there is a positive half-cycle current in phase A.

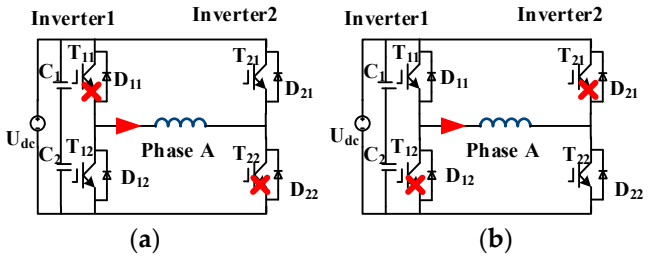


Figure 4. Two switches showing an open-circuit fault: (**a**) Open-circuit fault in T_{11} and T_{22}; and (**b**) Open-circuit fault in T_{12} and T_{21}.

2.2.3. Open-Circuit Faults in Three and Four Switches

When any three switches of the H-bridge power cell within phase A have open-circuit faults, there is no current existing in phase A. Similarly, when all four switches have open-circuit faults, the phase A current is also zero.

Based on the above analysis, when the faulty power switch is diagonally opposite the H-bridge power cell, the OW FPFTPM motor drives will show the same behavior and one

kind of faulty phase current type corresponds to multiple situations of open-switch faults. Therefore, the open-switch fault cannot be merely decided by the faulty phase current type.

3. Detection Method for the Open-Switch Fault

The open-switch fault detection of OW FPFTPM motor drives is divided into two levels, one is to identify the faulty phase and the other is to distinguish the faulty switch within the H-bridge power cell. The content of this paper focuses on the open-switch fault within one phase. The two levels are introduced separately below.

3.1. Determination of the Faulty Phase

Because the motor drives adopt high-performance closed-loop control, the feedback stator current can track the reference current in real time in normal operation. The five-phase current of the FPFTPM motor can be expressed as:

$$i_n(t) = I_m \sin\left(\omega t - (n-1)\frac{2\pi}{5}\right) \tag{1}$$

where n = 1 through to 5, corresponds to either A, B, C, D, or E five-phase, respectively, and the phase current does not contain a third harmonics current during normal operation. When an open-switch fault occurs, the residual of each phase current can be defined as

$$f_n(t) = i_{nref}(t) - i_{nm}(t) \tag{2}$$

where i_{nref} represents the reference current and i_{nm} represents the measured feedback current. $f_n = (f_1, f_2, f_3, f_4, f_5)$ corresponds to the residual current of each phase. During the normal operation, the residual could be guaranteed to be zero. When there is open-switch fault, the feedback current of the faulty phase becomes zero, or exists in the positive or negative half-cycle. When the faulty phase current exists in the negative half-cycle, the residual current is presented as:

$$f_n(t) = \begin{cases} I_m \sin\left(\omega t - (n-1)\frac{2\pi}{5}\right) & (n-1)\frac{2\pi}{5} \le \omega t \le (n-1)\frac{2\pi}{5} + \pi \\ 0 & \pi + (n-1)\frac{2\pi}{5} \le \omega t \le (n-1)\frac{2\pi}{5} + 2\pi \end{cases} \tag{3}$$

When the faulty phase current exists in the positive half-cycle, the residual current is presented as:

$$f_n(t) = \begin{cases} 0 & (n-1)\frac{2\pi}{5} \le \omega t \le (n-1)\frac{2\pi}{5} + \pi \\ I_m \sin\left(\omega t - (n-1)\frac{2\pi}{5}\right) & \pi + (n-1)\frac{2\pi}{5} \le \omega t \le (n-1)\frac{2\pi}{5} + 2\pi \end{cases} \tag{4}$$

The residual current f_n is transformed to the fundamental α-β plane and the third harmonic α_3-β_3 plane as:

$$\begin{aligned} \left[f_{\alpha\text{-}\beta}\right] &= \left[T_{\alpha\beta}\right]\left[f_n\right]^T \\ &= \left[i_{\alpha\beta ref}\right] - \left[i_{\alpha\beta m}\right] \\ \left[f_{\alpha 3\text{-}\beta 3}\right] &= \left[T_{\alpha 3\beta 3}\right]\left[i_{nref} - i_{nm}\right]^T \\ &= \left[i_{\alpha 3\beta 3 ref}\right] - \left[i_{\alpha 3\beta 3 m}\right] \\ f_0 &= i_{0ref} - i_{0m} \\ \left[T_{\alpha\text{-}\beta}\right] &= \frac{2}{5}\begin{bmatrix} 1 & \cos\alpha & \cos 2\alpha & \cos 3\alpha & \cos 4\alpha \\ 0 & \sin\alpha & \sin 2\alpha & \sin 3\alpha & \sin 4\alpha \end{bmatrix} \\ \left[T_{\alpha 3\text{-}\beta 3}\right] &= \frac{2}{5}\begin{bmatrix} 1 & \cos 3\alpha & \cos 6\alpha & \cos 9\alpha & \cos 12\alpha \\ 0 & \sin 3\alpha & \sin 6\alpha & \sin 9\alpha & \sin 12\alpha \end{bmatrix} \end{aligned} \tag{5}$$

where $\alpha = 0.4\pi$, $f_{\alpha\text{-}\beta}$, and $f_{\alpha 3\text{-}\beta 3}$ are the residual currents that belong to orthogonal subspaces, the α-β plane and the α_3-β_3 plane, and $i_{\alpha\beta ref}$ and $i_{\alpha\beta m}$ are the reference current and the measured current, respectively, in the α-β plane. Likewise, $i_{\alpha 3\beta 3ref}$ and $i_{\alpha 3\beta 3m}$ are the reference current and the measured current, respectively, in the α_3-β_3 plane. Moreover, i_{0ref} and i_{0m} are the reference zero-sequence current and the measured zero-sequence current, respectively. Since the back EMF of FPFTPM motors does not contain the third harmonic, the current component should be controlled only by existing in the α-β plane during normal operation. When an open-circuit fault occurs, the feedback current cannot dynamically follow the reference current and the phase current has a third harmonic component in the α_3-β_3 plane. As a result, the residual current appears in the third harmonic plane. The detection method proposed in this paper is based on the third harmonic residual current. In order to enhance the accuracy of the detection algorithm, a standardized vector, $f_{\alpha 3\beta 3N(t)}$, is defined and illustrated as follows:

$$f_{\alpha 3N}(t) = \left(\frac{1}{\left\| i_{sref} \right\|} - \frac{1}{\| i_{sm} \|} \right) i_{\alpha 3m} \quad f_{\beta 3N}(t) = \left(\frac{1}{\left\| i_{sref} \right\|} - \frac{1}{\| i_{sm} \|} \right) i_{\beta 3m} \tag{6}$$

where $\left\| i_{sref} \right\|$ and $\| i_{sm} \|$ represent the amplitude of the reference current and the feedback current in the stationary reference frame, respectively. Their expression is as follows:

$$\begin{aligned} \left\| i_{sref} \right\| &= \sqrt{i_{\alpha m}^2 + i_{\beta m}^2 + i_{\alpha 3ref}^2 + i_{\beta 3ref}^2 + i_{0ref}^2} \\ \| i_{sm} \| &= \sqrt{i_{\alpha m}^2 + i_{\beta m}^2 + i_{\alpha 3m}^2 + i_{\beta 3m}^2 + i_{0m}^2} \end{aligned} \tag{7}$$

To eliminate the influence of the fundamental current component, the reference current component in (7) is replaced by the measured current, and the residual current in stationary reference frame is introduced into the equation to obtain:

$$\begin{aligned} \left\| i_{sref} \right\| &= \sqrt{\left(i_{\alpha ref} - f_\alpha \right)^2 + \left(i_{\alpha ref} - f_\alpha \right)^2 + i_{\alpha 3ref}^2 + i_{\beta 3ref}^2 + i_{0ref}^2} \\ \| i_{sm} \| &= \sqrt{\left(i_{\alpha ref} - f_\alpha \right)^2 + \left(i_{\alpha ref} - f_\alpha \right)^2 + \left(i_{\alpha 3ref} - f_{\alpha 3} \right)^2 + \left(i_{\beta 3ref} - f_{\beta 3} \right)^2 + \left(i_{0ref} - i_{0m} \right)^2} \end{aligned} \tag{8}$$

Substitute (8) into (6) to get:

$$\begin{aligned} f_{\alpha 3N}(t) &= \frac{1}{K} \left(\frac{1}{\sqrt{\left(1 + \frac{i_{\alpha 3ref}^2 + i_{\beta 3ref}^2 + i_{0ref}^2}{K^2} \right)}} - \frac{1}{\sqrt{\left(1 + \frac{\left(i_{\alpha 3ref} - f_{\alpha 3} \right)^2 + \left(i_{\beta 3ref} - f_{\beta 3} \right)^2 + \left(i_{0ref} - i_{0m} \right)^2}{K^2} \right)}} \right) \times \left(i_{\alpha 3ref} - f_{\alpha 3} \right) \\ f_{\beta 3N}(t) &= \frac{1}{K} \left(\frac{1}{\sqrt{\left(1 + \frac{i_{\alpha 3ref}^2 + i_{\beta 3ref}^2 + i_{0ref}^2}{K^2} \right)}} - \frac{1}{\sqrt{\left(1 + \frac{\left(i_{\alpha 3ref} - f_{\alpha 3} \right)^2 + \left(i_{\beta 3ref} - f_{\beta 3} \right)^2 + \left(i_{0ref} - i_{0m} \right)^2}{K^2} \right)}} \right) \times \left(i_{\beta 3ref} - f_{\alpha 3} \right) \\ K &= \sqrt{\left(i_{\alpha ref} - f_\alpha \right)^2 + \left(i_{\alpha ref} - f_\alpha \right)^2} \end{aligned} \tag{9}$$

It can be concluded from (9) that $f_{\alpha 3N}$ and $f_{\beta 3N}$ are zero when the OW FPFTPM motor drives are in normal operation. Conversely, when an open-switch fault occurs, $f_{\alpha 3N}$ and $f_{\beta 3N}$ are no longer zero due to the appearance of the third harmonic current. According to (9), the trajectory of $f_{\alpha 3N}$ and $f_{\beta 3N}$ under an open-switch fault in phase B are presented in Figure 5. It can be concluded that the locus of ($f_{\alpha 3N}$ $f_{\beta 3N}$) shows different features

depending on the faulty phase current type. Therefore, the slope of the trajectory can be used to distinguish the faulty phase. When the open-switch fault occurred in the rest of the phases, the whole locus of ($f_{\alpha 3N}\, f_{\beta 3N}$) is shown in Figure 6. In the figure, the symbols '+' and '−' represent the faulty phase current existing in the positive half-cycle and the negative half-cycle, respectively.

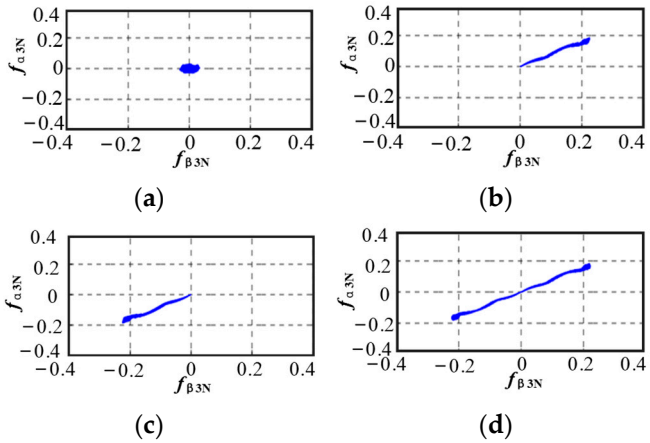


Figure 5. Locus of ($f_{\alpha 3N}\, f_{\beta 3N}$) when there is an open-switch fault in phase B: (**a**) Drives have no open-switch fault; (**b**) Negative half-cycle current; (**c**) Positive half-cycle current; and (**d**) Null current.

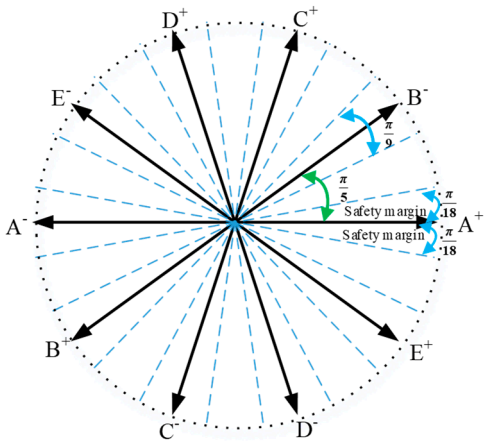


Figure 6. Locus of ($f_{\alpha 3N}\, f_{\beta 3N}$) according to different faulty phases.

According to the analysis of the ($f_{\alpha 3N}\, f_{\beta 3N}$), the identification of the faulty phase can be divided into two steps. Specifically, firstly checking whether there is an open-switch fault followed by the detection of the faulty phase. To determine the occurrence of the open-switch fault, the average amplitude $F_i(t)$ is defined as follows:

$$F_i(t) = \frac{1}{T(t)} \int_{t-T(t)}^{t} \left(f_{\alpha 3N}^2 + f_{\beta 3N}^2 \right)^{1/2} dt \tag{10}$$

where $T(t) = 2\pi/\omega$, and the dynamic window $[t - T(t); T(t)]$ is used to prevent false alarms and enhance the anti-interference performance of the detection algorithm. If the fault feature $F_i(t)$ is close to zero, the drives are in healthy states. However, if $F_i(t)$ exceeds the threshold of F_{th}, the drives have an open-switch fault. Therefore, the open-switch fault of the drives can be detected by $F_i(t)$.

The next step is to identify the faulty phase. As mentioned earlier, it can be achieved through the trajectory slope of ($f_{\alpha 3N}\, f_{\beta 3N}$). To accelerate the convergence speed and improve

the identification of the faulty phase, the least squares fitting method based on the forgetting factor is used for parameter identification. The specific formula is shown as follows:

$$\begin{aligned} K_k &= P_{k-1}H_k^T\left(H_kP_{k-1}H_k^T + \lambda R_k\right)^{-1} \\ \hat{x}_k &= \hat{x}_{k-1} + K_k\left(y_k - H_k\hat{x}_{k-1}\right) \\ P_k &= \lambda^{-1}(I - K_kH_k)P_{k-1} \end{aligned} \tag{11}$$

where k is the number of beats, H_k is the input data, corresponding to $f_{\alpha 3N}$, and y_k is the output data, corresponding to $f_{\beta 3N}$. P_k is the covariance, K_k is the gain coefficient, and $\hat{x}_k$ is the parameter to be identified. In particular, the choice of the forgetting factor, λ, is significant due to its influence on the convergence speed and tracking ability of the algorithm. In this study, λ is set to be 0.98, which not only ensures the rapid convergence of $\hat{x}_k$, but also prevents oscillation and reduces the tracking error. After $\hat{x}_k$ is identified, the angle of the trajectory slope is deduced as follows:

$$F_{PH} = \left\{ \begin{array}{ll} \arctan\hat{x}_k & if\ \hat{x}_k \geq 0 \\ \pi + \arctan\hat{x}_k & if\ \hat{x}_k < 0 \end{array} \right\} = (n-1)\frac{\pi}{5} \pm \frac{\pi}{18} \tag{12}$$

To enhance the anti-interference performance of the algorithm, $\pi/18$ is selected as the safety margin, as displayed in Figure 6. Through (12), the faulty phase can be identified. As the faulty current type is related to the open-switch fault, in order to identify the faulty phase current type, the average value of the faulty vector is defined as follows:

$$F_{\alpha 3N} = \frac{1}{T(t)}\int_{t-T(t)}^{T(t)} f_{\alpha 3N}dt \quad F_{\beta 3N} = \frac{1}{T(t)}\int_{t-T(t)}^{T(t)} f_{\beta 3N}dt \tag{13}$$

The faulty phase current type can be determined based on the average value of the residual vector $F_{\alpha 3N}$ and $F_{\beta 3N}$. In the different faulty phases, the faulty phase current type can be identified as shown in Table 3.

Table 3. Identification of The Faulty Phase Current Type.

Faulty Phase	$F_{\alpha 3N}$	$F_{\beta 3N}$	Faulty Phase Current Type
A	$F_{\alpha 3N} = 0$	$F_{\beta 3N} = 0$	Null current
	$F_{\alpha 3N} < 0$	$F_{\beta 3N} = 0$	Negative half-cycle current
	$F_{\alpha 3N} > 0$	$F_{\beta 3N} = 0$	Positive half-cycle current
B	$F_{\alpha 3N}$=0	$F_{\beta 3N} = 0$	Null current
	$F_{\alpha 3N} > 0$	$F_{\beta 3N} > 0$	Negative half-cycle current
	$F_{\alpha 3N} < 0$	$F_{\beta 3N} < 0$	Positive half-cycle current
C	$F_{\alpha 3N} = 0$	$F_{\beta 3N} = 0$	Null current
	$F_{\alpha 3N} < 0$	$F_{\beta 3N} < 0$	Negative half-cycle current
	$F_{\alpha 3N} > 0$	$F_{\beta 3N} > 0$	Positive half-cycle current
D	$F_{\alpha 3N} = 0$	$F_{\beta 3N} = 0$	Null current
	$F_{\alpha 3N} < 0$	$F_{\beta 3N} > 0$	Negative half-cycle current
	$F_{\alpha 3N} > 0$	$F_{\beta 3N} < 0$	Positive half-cycle current
E	$F_{\alpha 3N} = 0$	$F_{\beta 3N} = 0$	Null current
	$F_{\alpha 3N} < 0$	$F_{\beta 3N} > 0$	Negative half-cycle current
	$F_{\alpha 3N} > 0$	$F_{\beta 3N} < 0$	Positive half-cycle current

The flow chart of faulty phase detection is shown as Figure 7.

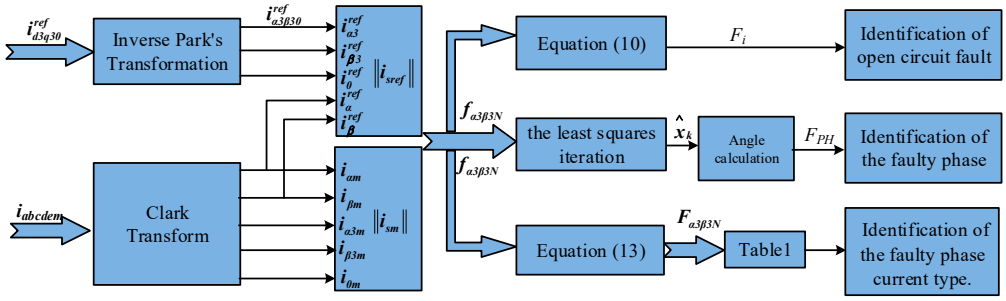


Figure 7. Flow chart of faulty phase detection.

3.2. Identification of the Faulty Switch within the H-Bridge Power Cell

In section A, after the identification of the faulty phase, the faulty phase current type can also be determined. However, one faulty phase current type is corresponding to several situations of open-switch fault within one H-bridge power cell. Therefore, in this section, an online current injection test method is proposed to accurately identify the open-circuit switches within one H-bridge power cell.

Given the distinctiveness of the H-bridge power cell, all four of the switches have an independent current flow path. When there is an open-switch fault in OW FPFTPM motor drives, the back EMF still exists in the faulty phase winding. It is noted that the back EMF can be used as the power supply for all four switches within the H-bridge power cell.

As the back EMF is an AC voltage signal, the four switches within the H-bridge will usually have a half-cycle to withstand the forward voltage of the back EMF. During this period, the switch can be controlled to turn on and the current will appear in the winding. Consequently, the reference-injection current can be set to be 180° phase shift with the back EMF, and the specific expression is as follows:

$$i_{n\,d}^{ref} = a\sin\left(\theta - (n-1)\frac{2\pi}{5}\right) \tag{14}$$

where n = 1, 2, 3, 4, and 5 representing phase A, B, C, D, and E, respectively, and 'a' represents the reference current amplitude of the faulty phase. Through the hysteresis current feedback control of the faulty phase, the switching sequence of the corresponding switch is obtained.

Take the phase A winding as an example, if phase A winding has a negative half-cycle current type, it can be deduced that the switches T_{21} and T_{12} must be healthy, and that at least one faulty switch exists in T_{11} and T_{22}. Therefore, it is necessary to conduct a current injection test on T_{11} and T_{22} to accurately identify the faulty switches.

During the first test of T_{11}, the remaining three switches are turned off through removing the gate signals of the three switches as shown in Figure 8a. The reference current of phase A is set according to (14), and the gate signals of T_{11} are obtained through the hysteresis controller. If T_{11} is healthy, the test current in phase A will follow the reference current. Otherwise, when T_{11} has an open-switch fault, the test current is always zero. The root mean square (RMS) and average (AVG) of the test current in phase A are used to determine whether T_{11} is faulty. If T_{11} is healthy, T_{22} must be faulty, and the test ends. If T_{11} has an open-switch fault, it is necessary to check T_{22}, and perform the second current injection test as revealed in Figure 8b. The test process of T_{22} is similar to T_{11}. The remaining three switches are actively disconnected except T_{22}, and the gate signals of T_{22} can also be obtained through the hysteresis controller. If T_{22} is healthy, the test current will follow the reference one. If T_{22} has an open-switch fault, the test current is always zero. So far, the accurate identification of the faulty switch can be completed through two current injection tests.

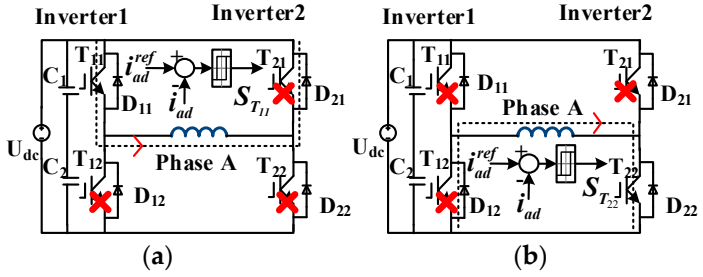


Figure 8. Identification procedure with the negative half-cycle current in phase A: (**a**) First test; and (**b**) Second test.

Likewise, if the faulty phase has the positive half-wave current as shown in Figure 9a,b, it can be inferred that T_{11} and T_{22} are in heathy states, and either T_{12} or T_{21} has an open -switch fault. In order to accurately identify the faulty switch, the current injection tests for T_{12} and T_{21} are similar to those for T_{11} and T_{22}. Accordingly, the RMS and AVG of the test current can be utilized to identify whether T_{11} is faulty.

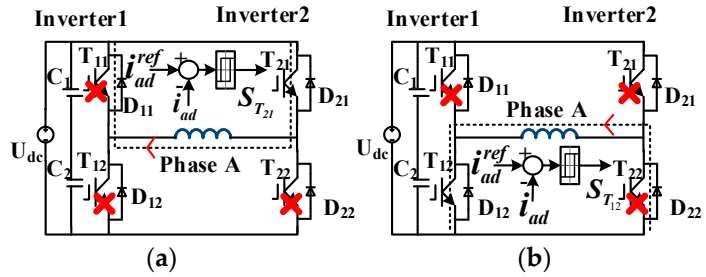


Figure 9. Identification procedure with the positive half-cycle current in phase A: (**a**) First test; and (**b**) Second test.

Next, when there is no current in the faulty phase A, there are nine possible open-switch fault situations. The current injection test method is shown in Figure 10. When the first current injection detection is performed, the gate signals of T_{12} and T_{22} are actively removed, and only T_{11} and T_{21} are left in the H-bridge power cell, as depicted in Figure 10a. When T_{11} withstands a forward voltage, T_{21} must withstand a reverse voltage. Conversely, when T_{21} bears a forward voltage, T_{11} must bear a reverse voltage. Therefore, the test current flow paths of the two switches are independent of each other in their respective half-current cycles. When T_{11} is turned on, a positive half-cycle test current will appear in phase A. When T_{21} is turned on, a negative half-cycle test current will appear in phase A. The gate signals of T_{11} and T_{21} can be obtained by the hysteresis controller. After the first current injection test, if the test current appears in phase A within one current cycle, then it can be determined that both T_{12} and T_{22} must have open-circuit faults, and the detection process ends. If the test current is a positive half-cycle current with amplitude 'a', it can be judged that T_{11} is healthy, T_{21} and T_{22} have open-switch faults, and only the state of T_{12} is unknown. Therefore, T_{12} needs to be tested separately, and the test process is the same as described in Figure 9b. If the test current is a negative half-cycle current, it can be judged that T_{21} is healthy, T_{11} and T_{12} have open-switch faults, and only the state of T_{22} is unknown. Therefore, T_{22} needs to be tested separately, and the test process is the same as described in Figure 8b. If there is no current in phase A during the current detection process, it indicates that both T_{11} and T_{21} have open-switch faults. The next step is to detect the states of T_{12} and T_{22}. The detection diagram is presented in Figure 10b. the figure shows that the gate signals of T_{12} and T_{22} can be obtained by the hysteresis controller. In all cases above, the RMS and AVG of the test current are used to determine whether the T_{12} and T_{22} are faulty, and the fault detection of all the switches is completed. The identification of the faulty switch within the H-bridge power cell is as shown in Figure 11.

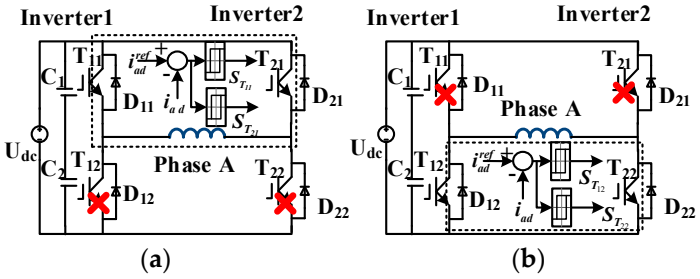


Figure 10. Identification procedure with no current in phase A: (**a**) First test; and (**b**) Second test.

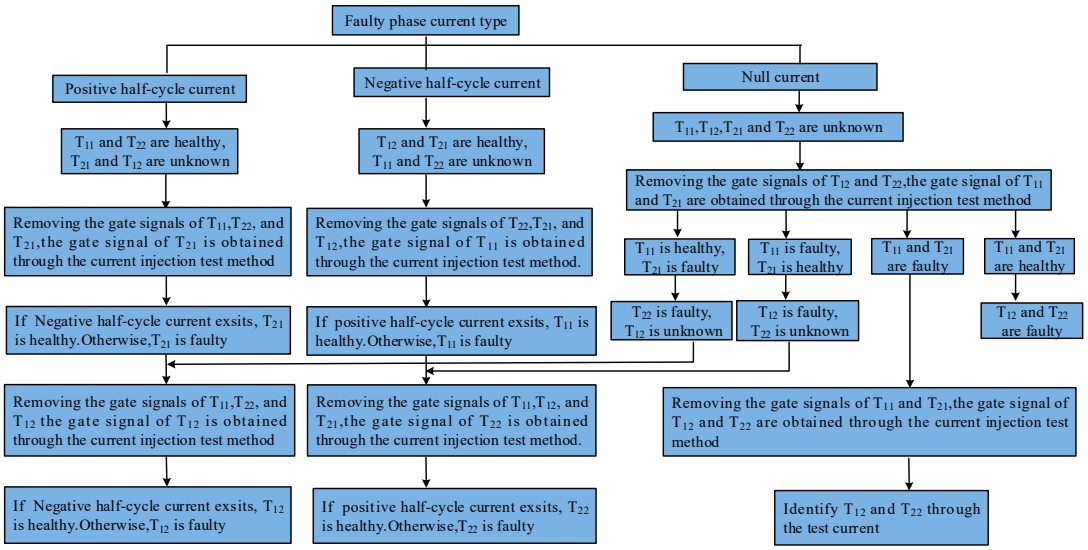


Figure 11. Identification of the faulty switch within the H-bridge power cell.

The reference test current is artificially set, having no correlation with the speed and load. Therefore, the influence of the speed and load on the test current can be eliminated, thereby reducing the false alarm. Additionally, when the open-switch fault occurs in other phases, the faulty switch identification procedure is similar to that for phase A.

4. Experimental Results and Discussion

4.1. Experimental Test Bench

To verify the effectiveness of the open-switch fault detection method proposed in this paper, an experimental test bench was built based on the DSP28377D processor as shown in Figure 12. The magnetic powder brake provides the required load to the drives, which is connected to the OW FPFTPM motor through the torque sensor. In addition, the power switches employed in inverter 1 and inverter 2 are insulated gate bipolar transistors (IGBT) with the switching sequence of 10 kHz. The speed during the experimental verification is 600 r/min and the torque is 4N·m. The threshold, F_{th}, of the diagnostic variables F_i, $F_{\alpha 3N}$, and $F_{\beta 3N}$ is set to be 5×10^{-3}. The angle error threshold, F_e, is set to be 10°, and the RMS and AVG threshold, I_{th}, of the test current is set to be 0.07. Additionally, the reference current amplitude 'a' during the current injection test is selected as 0.5 A.

4.2. Results and Discussion

Figure 13a presents the dynamic process from the normal operation to the occurrence of an open-switch fault in T_{11} of phase A and then to the current injection test. When T_{11} has an open-switch fault at t = 0.04 s, the faulty phase current only exists in the negative half-cycle, showing consistence with the analysis. With the value of the diagnostic variable, F_i, exceeding F_{th}, it can be judged that the drives have an open-switch fault. Next, the faulty phase A is determined by the faulty phase angle, F_{PH}. To avoid misjudgment, the

examination of the faulty phase is delayed for a half-cycle of the current. After the delay is over, F_{PH} is close to zero, and within plus or minus 10°.It is finally determined that the open-switch fault occurs in phase A. Since $|F_{\alpha 3N}| > F_{th}$, $F_{\beta 3N} = 0$, it can be inferred from Table 3 that the faulty phase has a negative half-cycle current and the switches T_{12} and T_{21} are healthy.

Consequently, either the switch T_{11} or T_{22} has an open-switch fault and the current injection test is further required. The current injection test is carried out twice and each test time is one current cycle. Once the half-current cycle delay is over, the current injection test is applied according to Figure 9. When the first test is performed, the gate signals of T_{22}, T_{21}, and T_{12} are removed, and the gate signal of T_{11} is obtained through the current controller. The RMS and AVG of the test current are close to zero and it can be determined that T_{11} has an open-switch fault. When performing the second test, the gate signals of T_{22}, T_{21}, and T_{12} are removed, and gate signal of T_{11} is obtained through the current controller. The RMS and AVG of the test current are close to 0.25 and 0.16, respectively. It can be inferred that T_{22} is healthy and that the entire single open-switch fault detection process has been completed. When the faulty phase has a negative half-cycle current, two current injection tests are also required, and the detection process is shown in Figure 8.

Figure 13b shows the experimental results when the diagonally opposite switches T_{14} and T_{23} in phase B have open-switch faults. This shows that the faulty current of phase B exists in the positive half-cycle. After a current cycle, the diagnostic variable F_i detects the occurrence of the open-switch fault, and $F_{PH} = 40°$ determines that the faulty phase is B as revealed in Figure 13b. Compared with Figure 13a, F_{PH} changed significantly. When the open-circuit fault occurs in other phases, F_{PH} is shown as in Figure 6. Then, the average fault vector $|F_{\alpha 3N}| > F_{th}$, $|F_{\beta 3N}| > F_{th}$ notes that the faulty phase current type is a positive half-cycle waveform, indicating that T_{13} and T_{24} are healthy. According to Figure 9, two current injection tests are required. In the first test, the gate signals of T_{13}, T_{23}, and T_{24} are removed, and the gate signal of T_{14} is obtained through the current controller; in the second test, the gate signals of T_{13}, T_{14}, and T_{24} are removed, and the gate signal of T_{23} is obtained through the current controller. In both tests, the RMS and AVG of the test current are zero, which means T_{14} and T_{23} have open-circuit faults.

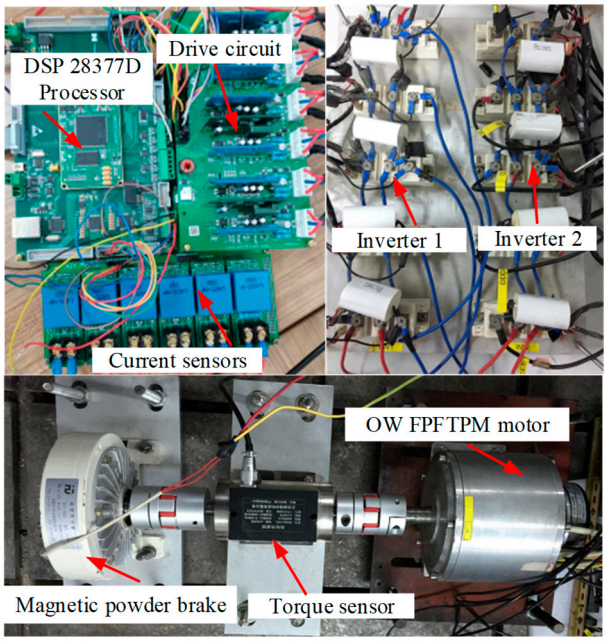


Figure 12. Experimental test bench.

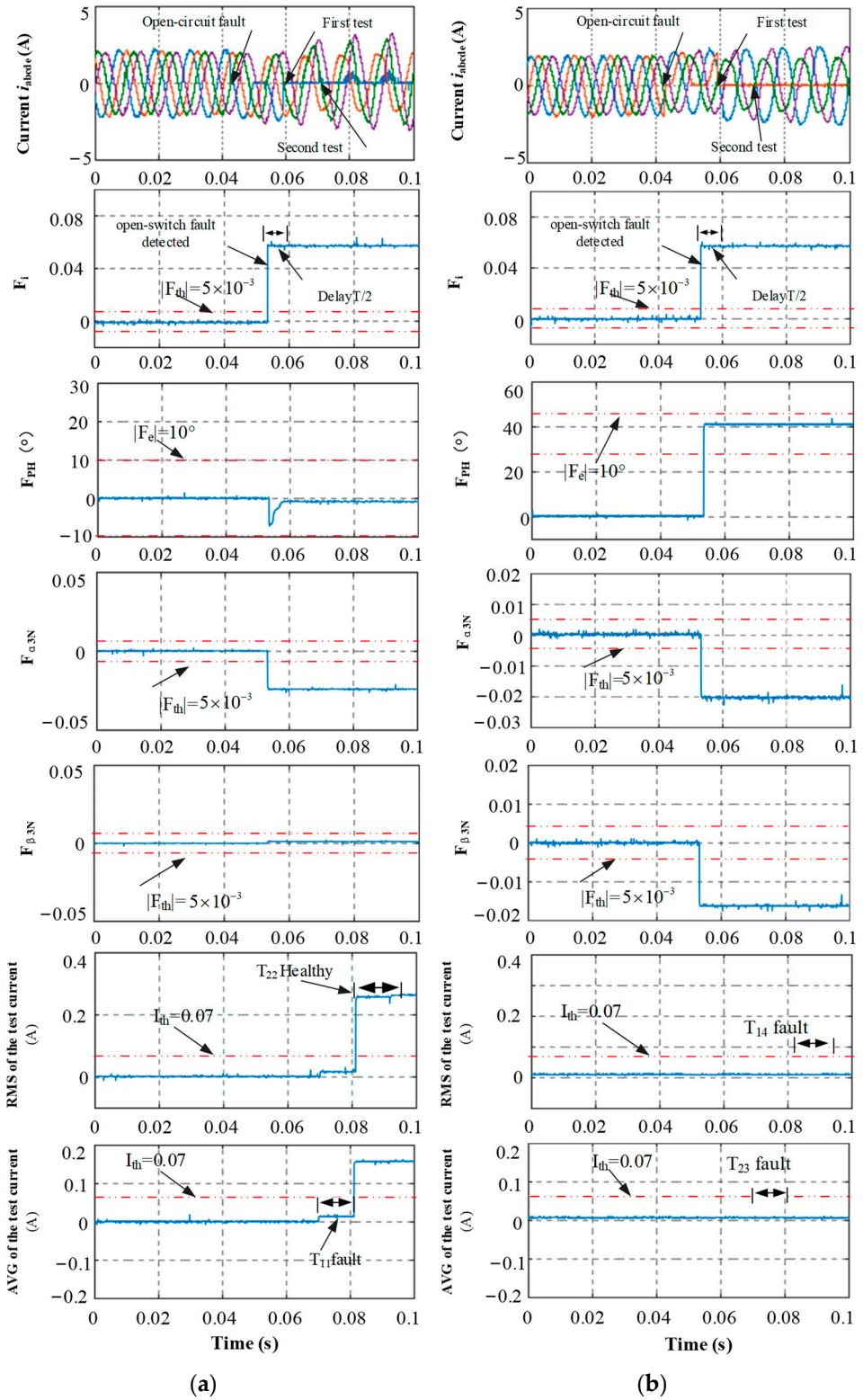


Figure 13. Experimental results: the blue line represents the diagnostic variable, and the red line represents the threshold of amplitude. (**a**) T_{11} with an open-circuit fault in phase A; and (**b**) T_{14} and T_{23} with an open-circuit fault in phase B.

Figure 14a demonstrates the experimental results when the three switches T_{13}, T_{14}, and T_{23} of phase B have open-switch faults. F_{PH} indicates that phase B suffers from open-circuit fault. Furthermore, it is observed that the faulty phase current type is zero. Based on the

faulty phase current type, the current injection test is conducted as described in Figure 10. In the first test, the gate signals of T_{14} and T_{24} are removed, and gate signal of T_{13} and T_{23} are obtained through the current controller; and the first test indicates that T_{13} and T_{23} have open-switch faults as the test current is zero. In the second test, the gate signals of T_{13} and T_{23} are removed, and gate signal of T_{14} and T_{24} are obtained through the current controller, and the second test shows the AVG and RMS of the test current are 0.25 and 0.16, respectively, which means T_{24} is healthy and T_{14} is the faulty switch. The experimental results show that the detection method can effectively detect the open-switch fault in the case of three switches.

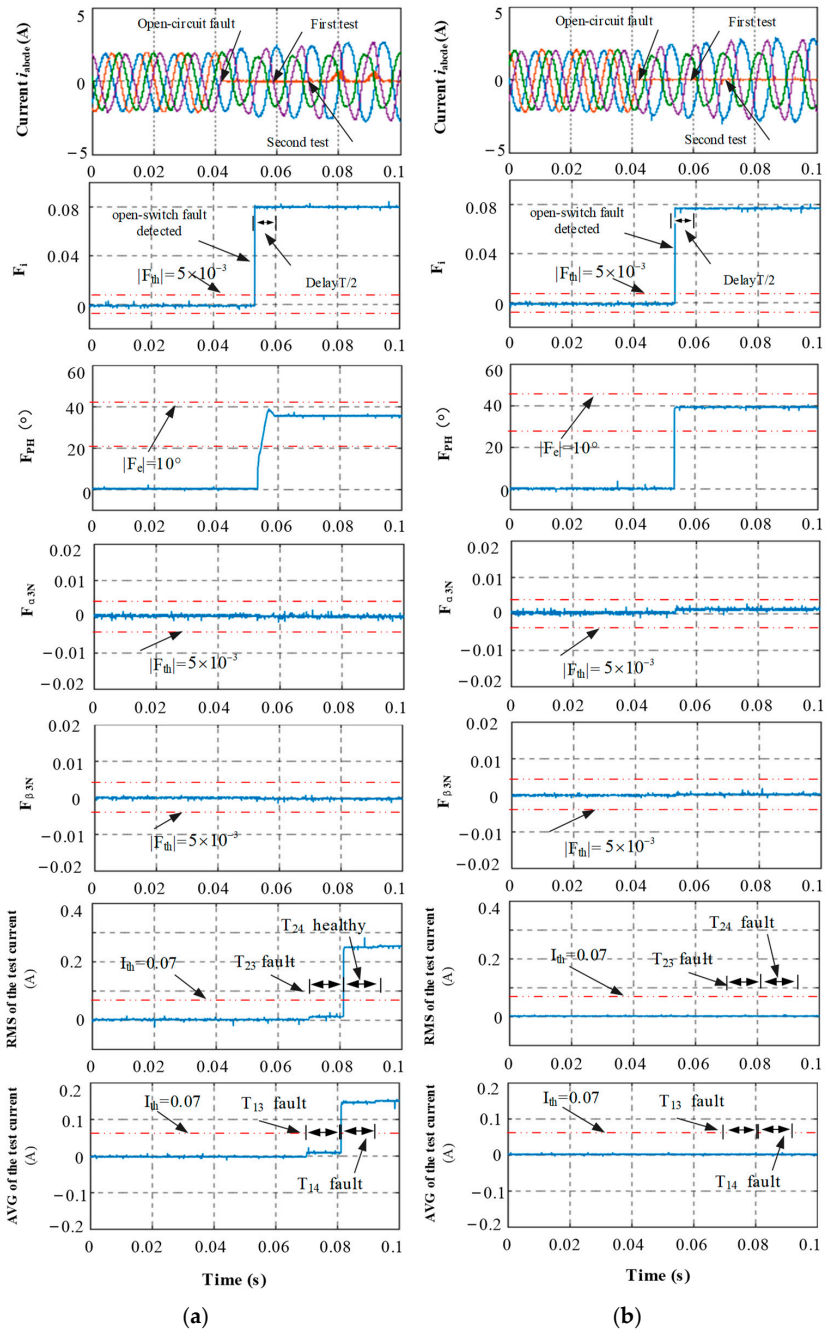


Figure 14. Experimental results: the blue line represents the diagnostic variable, and the red line represents the threshold of amplitude. (**a**) T_{13}, T_{14}, and T_{23} with an open-circuit fault in phase B; and (**b**) All the four switches with an open-circuit fault in phase B.

When all four switches in phase B have open-switch faults, the experimental results are shown in Figure 14b. In this case, from the occurrence of the fault to the current injection test, there is no current in phase B, and the diagnostic variables F_i, $F_{\alpha 3N}$, $F_{\beta 3N}$, and F_{PH} are similar to those in Figure 14a. Then, based on the AVG and RMS of the test current, it is noted that T_{13}, T_{23}, T_{14}, and T_{24} of phase B have open-circuit faults.

To further verify the anti-interference performance of the detection method under normal operation proposed in this article, Figure 15 reveals the experimental results when the speed changes from 300 r/min to 600 r/min. It is evident from Figure 15, that both the amplitude and frequency of the current have changed. During transient states, the diagnostic variables F_i, $F_{\alpha 3N}$, and $F_{\beta 3N}$ have been kept within the normal bands. The above experimental results verify that the detection method proposed in this paper has a robust performance during the transient variation of the load and speed.

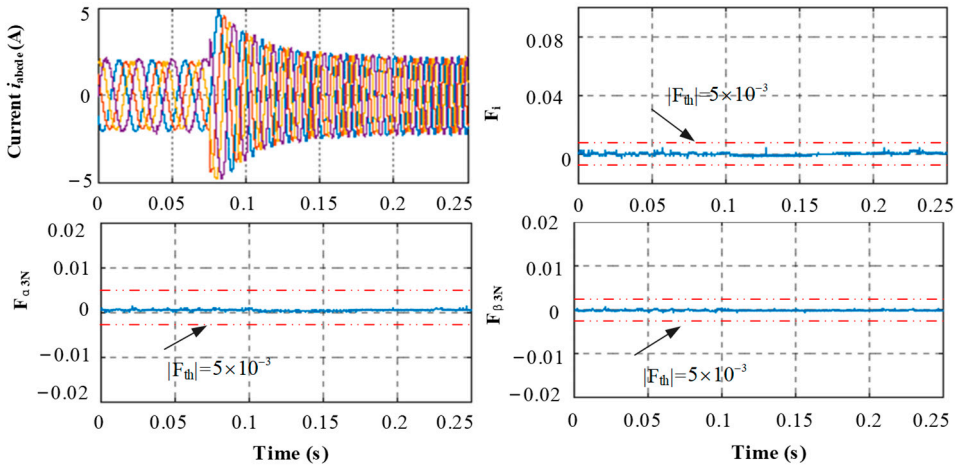


Figure 15. Experimental results during the variable speed dynamic process (the blue line represents the diagnostic variable, and the red line represents the threshold of amplitude).

4.3. Key Findings of the Detection Method

In the present study, an open-switch fault detection method based on open-winding OW FPFTPM motor drives is proposed to solve the problem that the fault at the diagonally opposite position within the H-bridge power cell shares the same fault characteristics. Some key findings of the detection method are presented as follows:

(1) The back EMF can be used as the power supply. Combined with the characteristics of the OW structure, the current injection test can be used to identify the open-switch fault;
(2) Compared with the conventional detection method, the proposed method can extract detailed open-switch fault information online within one half-current cycle, including the fault phase, the fault current type, and the fault switch position. Based on the extracted information, the drives can easily realize fault-tolerant control under the open-switch fault;
(3) The detection method uses the residual of the third harmonic current for fault detection, so it is not affected by the variable of motor load. Furthermore, this method does not require additional sensors and additional circuits, thus reducing the detection cost, which is suitable for engineering applications.

5. Conclusions

This paper proposed an online open-switch fault detection method based on OW FPFTPM motor drives, which can accurately identify the faulty phase and the faulty switches of the H-bridge power cell within one phase. During the fault detection, the residual vector of the third harmonic current and the least square method based on the forgetting factor are used to detect the faulty phase and the faulty current type. In addition, to accurately identify the faulty switches within one phase, a current injection test method is

proposed. This method mainly uses the back EMF of the faulty phase winding as excitation and applies a gate signal to the test switches within the H-bridge power cell. The gate signals can be obtained by a hysteresis controller, and the state of each switch within the H-bridge power cell can be accurately identified by the AVG and RMS of the test current in the faulty phase. The proposed detection method does not require additional sensors apart from the current sensors, which are already provided for the current measurements. Furthermore, the experimental results for OW FPFTPM motor drives are presented in order to evaluate the proposed detection method.

Author Contributions: Conceptualization, R.C. and S.Y.; methodology, R.C.; software, R.C.; validation, R.C., S.Y. and S.L.; formal analysis, R.C.; investigation, R.C.; resources, R.C.; data curation, R.C.; writing—original draft preparation, R.C.; writing—review and editing, S.Y. and S.L.; visualization, R.C.; supervision, S.Y. and S.L.; project administration, R.C.; funding acquisition, R.C. and S.Y. All authors have read and agreed to the published version of the manuscript.

Funding: This research was supported in part by the Natural Science Foundation of the Jiangsu Higher Education Institutions of China (grant number 22KJB470026) and the Lv Yang Jin Feng Program of Yangzhou (grant number YZLYJFJH2021YXBS130).

Data Availability Statement: Not applicable.

Conflicts of Interest: The authors declare no conflict of interest.

Notations

i_{nref}	The reference current
i_{nm}	The measured feedback current
f_n	The residual current of each phase
$f_{\alpha\text{-}\beta}$	The residual current in the α-β plane
$f_{\alpha 3\text{-}\beta 3}$	The residual current in the α_3-β_3 plane
$i_{\alpha\beta ref}$	The reference current in the α_3-β_3 plane
$i_{\alpha 3\beta 3m}$	The measured current in the α_3-β_3 plane
i_{0ref}	The reference zero-sequence current
i_{0m}	The measured zero-sequence current
$\left\|i_{sref}\right\|$	The amplitude of the reference current in the stationary reference frame
$\|i_{sm}\|$	The amplitude of the feedback current in the stationary reference frame
$f_{\alpha 3N}$	The fault feature in α_3-axis
$f_{\beta 3N}$	The fault feature in β_3-axis
F_i	Magnitude of the fault feature in the α_3-β_3 plane
H_k	The input data
y_k	The output data
P_k	The covariance
K_k	The gain coefficient
λ	The forgetting factor
F_{PH}	The angle of the faulty phase
$F_{\alpha 3N}$	The average value of $f_{\alpha 3N}$
$F_{\beta 3N}$	The average value of $f_{\beta 3N}$
i_{nd}^{ref}	The reference current amplitude of the faulty phase

References

1. Kim, H.; Lee, C. Shape parameters design for improving energy efficiency of IPM traction motor for EV. *IEEE Trans. Veh. Technol.* **2021**, *70*, 6662–6673. [CrossRef]
2. Razi, M.; Murgovski, N.; McKelvey, T.; Wik, T. Design and comparative analyses of optimal feedback controllers for hybrid electric vehicles. *IEEE Trans. Veh. Technol.* **2021**, *70*, 2979–2993. [CrossRef]
3. Jung, S.; Ko, J.J. Study on regenerative energy recovery of electric vehicle through voltage control using switched capacitor. *IEEE Trans. Veh. Technol.* **2021**, *70*, 4324–4339. [CrossRef]
4. Shi, Z.; Sun, X.; Cai, Y.; Yang, Z. Robust design optimization of a five-phase PM hub motor for fault-tolerant operation based on taguchi method. *IEEE Trans. Energy Convers.* **2020**, *35*, 2036–2044. [CrossRef]

5. Lin, H.; Zhao, F.; Kwon, B. Analysis and control of the permanent magnet synchronous motor with auxiliary modular design. *IEEE Trans. Magn.* **2018**, *54*, 8208206. [CrossRef]
6. Zhang, L.; Zhu, X.; Gao, J.; Mao, Y. Design and analysis of new five-phase flux-intensifying fault-tolerant interior-permanent-magnet motor for sensorless operation. *IEEE Trans. Ind. Electron.* **2020**, *67*, 6055–6065. [CrossRef]
7. Zhou, H.; Zhou, C.; Tao, W.; Wang, J.; Liu, G. Virtual-stator-flux-based direct torque control of five-phase fault-tolerant permanent-magnet motor with open-circuit fault. *IEEE Trans. Power Electron.* **2020**, *35*, 5007–5017. [CrossRef]
8. Priestley, M.; Fletcher, J.; Tan, C. Space-vector PWM technique for five-phase open-end winding PMSM drive operating in the overmodulation region. *IEEE Trans. Ind. Electron.* **2018**, *65*, 6816–6827. [CrossRef]
9. Belkhode, S.; Jain, S. Optimized switching PWM technique with common-mode current minimization for five-Phase open-end winding induction motor drives. *IEEE Trans. Power Electron.* **2019**, *34*, 8971–8980. [CrossRef]
10. Priestley, M.; Farshadnia, M.; Fletcher, J. FOC transformation for single open-phase faults in the five-phase open-end winding topology. *IEEE Trans. Ind. Electron.* **2020**, *67*, 842–851. [CrossRef]
11. Jlassi, I.; Cardoso, A. A single method for multiple IGBT, current, and speed sensor faults diagnosis in regenerative PMSM drives. *IEEE J. Emerg. Sel. Top. Power Electron.* **2020**, *8*, 2583–2599. [CrossRef]
12. Mazzoletti, M.; Bossio, G.; Angelo, C.; Espinoza-Trejo, D. A model-based strategy for interturn short-circuit fault diagnosis in PMSM. *IEEE Trans. Ind. Electron.* **2017**, *64*, 7218–7228. [CrossRef]
13. Gonz'alez-Prieto, I.; Duran, M.; Rios-Garcia, N.; Barrero, F.; Mart´ın, C. Open-switch fault detection in five-phase induction motor drives using model predictive control. *IEEE Trans. Ind. Electron.* **2018**, *65*, 3045–3055. [CrossRef]
14. Khil, S.; Jlassi, I.; Cardoso, A.; Estima, J.; Mrabet-Bellaaj, N. Diagnosis of open-switch and current sensor faults in PMSM drives through stator current analysis. *IEEE Trans. Ind. Appl.* **2019**, *55*, 5925–5937. [CrossRef]
15. Shi, T.; He, Y.; Wang, T.; Tong, J.; Li, B.; Deng, F. An improved open-switch fault diagnosis technique of a PWM voltage source rectifier based on current distortion. *IEEE Trans. Power Electron.* **2019**, *34*, 12212–12225. [CrossRef]
16. Cheng, Y.; Sun, Y.; Li, X.; Dan, H.; Lin, J.; Su, M. Active common-mode voltage-based open-switch fault diagnosis of inverters in IM-drive systems. *IEEE Trans. Ind. Electron.* **2021**, *68*, 103–115. [CrossRef]
17. Hang, J.; Zhang, J.; Cheng, M.; Ding, S. Detection and discrimination of open-phase fault in permanent magnet synchronous motor drive system. *IEEE Trans. Power Electron.* **2016**, *31*, 4697–4709. [CrossRef]
18. Lamb, J.; Mirafzal, B. Open-circuit IGBT fault detection and location isolation for cascaded multilevel converters. *IEEE Trans. Ind. Electron.* **2017**, *64*, 4846–4856. [CrossRef]
19. Wu, X.; Chen, C.; Chen, T.; Cheng, S.; Mao, Z.; Yu, T.; Li, K. A fast and robust diagnostic method for multiple open-circuit faults of voltage-source inverters through line voltage magnitudes analysis. *IEEE Trans. Power Electron.* **2020**, *35*, 5205–5220. [CrossRef]
20. Shahin, A.; Martin, J.; Pierfederici, S. Zero-sequence current based diagnostic method for open-switch fault detection in parallel inverters system. *IEEE Trans. Power Electron.* **2019**, *34*, 3750–3764. [CrossRef]
21. Guo, H.; Guo, S.; Xu, J.; Tian, X. Power switch open-circuit fault diagnosis of six-phase fault tolerant permanent magnet synchronous motor system under normal and fault-tolerant operation conditions using the average current park's vector approach. *IEEE Trans. Power Electron.* **2021**, *36*, 2641–2660. [CrossRef]
22. Kong, J.; Wang, K.; Zhang, J.; Zhang, H. Multiple open-switch fault diagnosis for five-phase permanent magnet machine utilizing currents in stationary reference frame. *IEEE Trans. Energy Convers.* **2021**, *36*, 314–324. [CrossRef]
23. Salehifar, M.; Arashloo, R.; Equilaz, J.; Sala, V.; Romeral, L. Fault detection and fault tolerant operation of a five phase PM motor drive using adaptive model identification approach. *IEEE J. Emerg. Sel. Top. Power Electron* **2014**, *2*, 212–223. [CrossRef]
24. Trabelsi, M.; Semail, E.; Nguyen, N. Experimental investigation of inverter open-circuit fault diagnosis for biharmonic five-phase permanent magnet drive. *IEEE J. Emerg. Sel. Top. Power Electron.* **2018**, *6*, 339–351. [CrossRef]
25. Trabelsi, M.; Nguyen, N.; Semail, E. Real-time switches fault diagnosis based on typical operating characteristics of five-phase permanent-magnetic synchronous machines. *IEEE Trans. Ind. Electron.* **2016**, *63*, 4683–4694. [CrossRef]
26. Li, Z.; He, Y.; Gao, Y.; Zhang, X.; Wang, B.; Ma, H. A Model-Data-Hybrid-Driven diagnosis method for Open-Switch faults in power converters. *IEEE Trans. Power Electron.* **2021**, *36*, 4965–4970. [CrossRef]
27. Abari, I.; Hamouda, M.; Sleiman, M.; Slama, H.; Kanaan, Y.; AI-Haddad, K. Open-Circuit fault detection and isolation method for Five-Level PUC inverter based on the Wavelet Packet Transform of the radiated magnetic field. *IEEE Trans. Instrum. Meas.* **2022**, *71*, 3502611. [CrossRef]
28. Yan, H.; Xu, Y.; Cai, F.; Zhang, H.; Zhao, W.; Gerada, C. PWM-VSI fault diagnosis for a PMSM drive based on the fuzzy logic approach. *IEEE Trans. Power Electron.* **2019**, *34*, 759–768. [CrossRef]